ISSN 1062-8738, Bulletin of the Russian Academy of Sciences: Physics, 2023, Vol. 87, No. 11, pp. 1594–1600. © Pleiades Publishing, Ltd., 2023.
Russian Text © The Author(s), 2023, published in Izvestiya Rossiiskoi Akademii Nauk, Seriya Fizicheskaya, 2023, Vol. 87, No. 11, pp. 1562–1568.

Shear Strength of Al–Cu Alloys with Different Types of Hardening Precipitates: Molecular Dynamics and Continuum Modeling

P. A. Bezborodova[a, *], V. S. Krasnikov[a], M. R. Gazizov[b], A. E. Mayer[a], and V. V. Pogorelko[a]

[a] *Chelyabinsk State University, Chelyabinsk, 454001 Russia*

[b] *Belgorod State National Research University, Belgorod, 308015 Russia*

**e-mail: ibragimova-polin@mail.ru*

Received May 22, 2023; revised June 19, 2023; accepted July 28, 2023

Abstract—Molecular dynamics is used to study the motion of dislocations in aluminum containing hardening copper precipitates. The interaction between a dislocation and four experimentally observed types of precipitates is considered. The energy of dislocation segments attached to hardening phases is determined and used as a parameter in the continuum model of dislocation–precipitate interaction.

Keywords: Al–Cu alloy, molecular dynamics, hardening precipitate, dislocation, shear strength

DOI: 10.3103/S1062873823703744

INTRODUCTION

Aluminum alloys are widely used as structural materials in many areas of human activity. The high specific strength of aluminum alloys is achieved through heat treatment due to the formation of hardening phases during the migration of dissolved atoms of alloying elements [1]. In addition to precipitates of various phases, real alloys are known to contain other violations of the crystal lattice. Such point and extended defects as vacancies, dislocations, and grain boundaries, are observed in their structures. The motion of linear defects (dislocations that are the edges of atomic half-planes) largely determines the features of plastic deformation [2]. Hardening occurs when intermetallic precipitates act as barriers to the movement of dislocations [3, 4]. When precipitations of second phases facilitate the movement of dislocations, the alloy becomes brittle or weakens.

The sequence of the precipitation of hardening phases as an alloy ages obeys the scheme of supersaturated solid solution $\rightarrow$ GP1 $\rightarrow$ GP2 $\rightarrow$ θ'' $\rightarrow$ θ' $\rightarrow$ θ [5]. At the initial stage of heat treatment, copper atoms in a chaotic order collect in certain places of the aluminum matrix, forming structured precipitates (Guinier–Preston (GP) zones of the first and second types) [6]. The GP zones take the form of thin disc-shaped inclusions several atomic layers thick and 5–100 nm in diameter. The first type of GP zone is a copper disk surrounded by an aluminum matrix. Further heat treatment produces a second type of GP zones that consist of two parallel copper layers separated by three layers of aluminum atoms. The structure of θ'' phases is equivalent to GP2 zones, but consists of three or more copper atomic layers. After precipitation of the θ'' phase, there is a transformation into phase θ' during subsequent heat treatment. The θ' phase is the most important hardening precipitate in Al–Cu alloys. It has a tetragonal lattice $\left(I\bar{4}m2\right)$ with parameters a = 4.04 Å and c = 5.80 Å. The precipitates of the listed types are parallel to plane $(100)_{Al}$. Upon further aging, a completely incoherent θ phase forms in the melt, for which a great many possible conjugations of the lattice of precipitates and matrix are possible [7].

The development of electron microscopy allows us to study the atomic structure of hardening precipitates with nanometer resolution. Analysis of the resulting images shows there are more complex types of lattices of hardening precipitates than in the traditionally considered sequence of hardening phases [8–11]. The authors of [12] obtained a detailed image of the θ' phase with alternating aluminum and copper atoms at the interface. Structures with GP-like layers at the interface of θ' were detected experimentally in [13]. We can see from the micrographs in [14] that the θ' phase can have elongated layers of copper atoms along broad interfaces, in contrast to the internal structure.

Since the interaction between dislocations and hardening precipitates largely determines the mechanical properties of alloys, and the features of the crystal structure of inclusions affect their resistance to shear during interaction with a dislocation, it is important to study the relationship between structure and shear resistance. The development of atomistic modeling

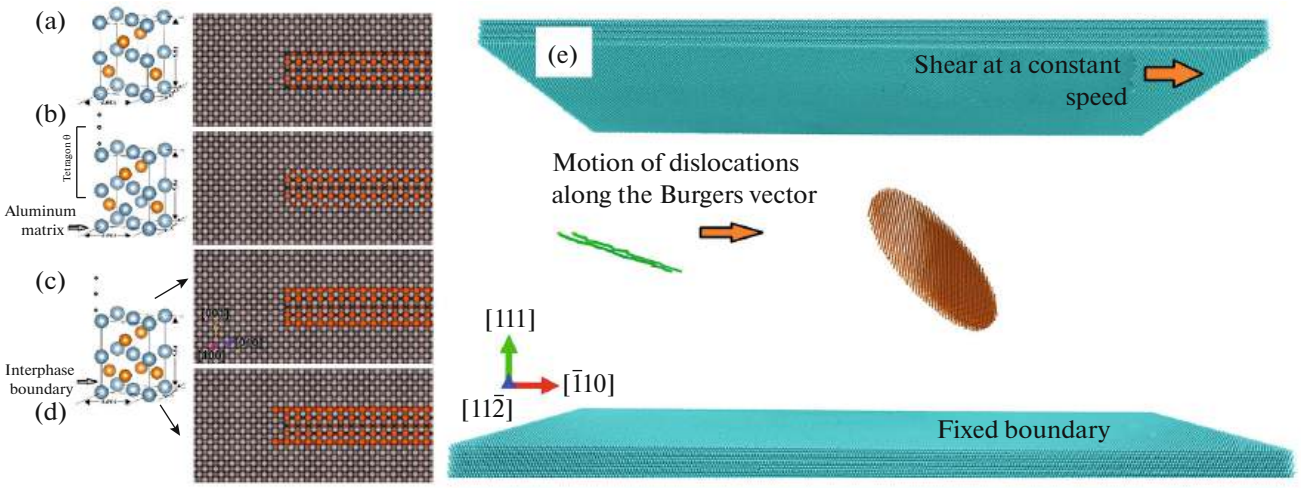

Fig. 1. Unit cells and inclusions in an aluminum matrix: (a) s-θ', (b) f-θ', (c) h-θ' and (d) (h + r)-θ'. (e) Computational domain and mutual orientation of a dislocation and a precipitate of phase θ'.

allows us to study the interaction between a dislocation and a hardening precipitate, which determines the main mechanisms of interaction for a particular type of precipitates and the numerical characteristics of this process. In the last decade, atomistic modeling has been used to study the interaction between dislocations and precipitates in alloys of various compositions [8, 15–19].

Atomistic modeling allows us to study in detail the dislocation-precipitate interction, but they have limitations in scales of space and time. To overcome these limitations, we use multiscale means that combine atomistic and continuum modeling. A way of reproducing the flow stress of an alloy was proposed in [8, 15–17] that includes atomistic modeling, continuum modeling of dislocation-precipitate interaction, and the dynamics of discrete dislocation. Results obtained in a multiscale study are in good agreement with experimentally measured flow stresses of aluminum alloys. However, hardening precipitates of the classical sequence of the Al–Cu system were considered in all the cited works. In this work, we used MD calculations to study the effect the crystal structure of θ'-phase-like precipitates has on their resistance to shear during interaction with a dislocation. The calculations were compared to MD data to determine continuum model parameters of the dislocation-precipitate interaction of four types.

MD INVESTIGATION OF DISLOCATION-PRECIPITATE INTERACTION

The unit cell of the θ'-phase contains Al and Cu atoms in the corresponding positions (Figs. 1a–1d). An important feature of the θ' phase lattice is planes with square lattices of atoms and parameters close to those of the aluminum matrix. There is coherent coupling with the aluminum matrix along these planes. The θ' lattice and the aluminum matrix are incommensurate along other planes where layers of copper atoms are observed, and interfaces form. For comparison, Figs. 1a–1d show the unit cells of other types of the θ' phases observed in experiments.

Precipitates were created on the basis of a unit cell using the Atomsk program [20]. They were 20 nm in diameter and 9 atomic layers wide, which corresponds to data observed experimentally. The first type (s) is a single-phase structure with a tetragonal lattice. The second type (f) is a structure with segregated aluminum atoms at the interface between copper atoms. The fcc order of atoms is also preserved at the interface. The third type (h) has a sandwich structure with a tetragonal θ' lattice in the core and GP-like structures along broad interfaces. The fourth type of structure, (h + r), is a θ' structure with GP interlayers at the interfaces. It has an additional monatomic copper layer in the form of a rim at the interfaces. The structures of precipitates built into the aluminum matrix are shown in Figs. 1a–1d.

Table 1. Energy of interaction between dislocations and precipitates in models with different temperatures

T, K	$\varepsilon^{p}_{s\text{-}\theta'}$, eV/b	$\varepsilon^{p}_{f\text{-}\theta'}$, eV/b	$\varepsilon^{p}_{h\text{-}\theta'}$, eV/b	$\varepsilon^{p}_{(h+r)\text{-}\theta'}$, eV/b
100	1.07	1.12	1.2	1.3
300	0.8	0.96	1.1	1.23
500	0.7	0.78	0.95	1.05
700	0.67	0.67	0.85	0.9

The resulting inclusions have a cylindrical form with bases parallel to plane (100) of the aluminum lattice. Since the θ' phase is commensurate with plane (100), the initial axes of the atomic system are oriented along crystallographic directions [100], [010] and [001]. The motion of dislocations and their interaction with θ'-phases are studied according to the scheme proposed in [21] for the slip system $[\bar{1}10](111)$, which is typical of fcc metals. The axes of the coordinate system used to study the motion of a dislocation are oriented along the crystallographic directions. Axis x is oriented in accordance with crystallographic direction $[\bar{1}10]$, the y axis is directed along direction [111], and axis z is directed along direction $[11\bar{2}]$. With this orientation, axis x is directed along the Burgers vector of an ideal edge dislocation, axis z is directed along the tangential vector of dislocation, and axis y is perpendicular to the slip plane. In a system containing 9000000 atoms with a volume of $77 \times 60 \times 32$ nm^3, periodic boundary conditions are set in the directions of the axes x and z, and nonperiodic boundary conditions are set along axis y. A dislocation is created in the computational domain by adding an additional atomic half-plane. At the initial moment, this ideal line of dislocation is directed along axis z, and the Burgers vector is directed along axis x of the coordinate system. The motion of a dislocation in a crystal arises due to external shear deformations. Shear deformation of the system occurs when the upper layer of atoms five interatomic distances thick shifts relative to the x axis at a constant rate of 4.2×10^7 s^{-1}, while the lower layer of atoms with the same thickness remains immobile (Fig. 1e). An NVE ensemble of particles was used to model the deformation of the system, and the temperature was maintained by a Berendsen thermostat [22]. MD calculations were made using the LAMMPS software package [23]. The deformation of the system continued for approximately ten interactions between the dislocation and an obstacle. The interaction beteen atoms was described using the ADP potential [24]. The potential reproduces the elastic constants and energies of various defects in both metals and intermetallic phases. The resulting atomic distributions were analyzed and visualized using the OVITO package [25].

The interactions between a dislocation and a precipitate produce sawtooth dependences of the volume-averaged shear stress of the system vs. time, as we can see in Figs. 2a–2d. After the first interaction, each peak corresponds to that of a dislocation which passed through a periodic border with a precipitate. Our calculated results were compared statistically for a temperature of 300 K. Slight deviation of the stress levels for subsequent interactions is shown in Figs. 2a, 2c. The initial distributions of the velocity of atoms differed at each run of MD modeling, though they had the same temperature of the entire system. It should be noted that there are two clearly distinguishable stress levels for the first interaction between the two types of precipitates. This is due to a negligible difference between the mechanism of the first interaction of dislocation and both types of inclusions. Let us consider the difference using the s-θ' interaction as an example. The mechanism of Orowan interaction described in [26] is observed for a section with a lower level of stress on the curve. The dislocation segment bypassing the precipitate moves along its back side, creating the classical Orowan mechanism. With a higher level of stress on the plot, the dislocation in the system shifts to the neighboring slip plane. A fluctuation arising on the elongated segment of dislocation results in ejection of the helical segment of dislocation into the adjacent slip plane. An additional segment then forms that connects segments dislocations in neighboring slip planes. This raises the energy costs and shear stress when overcoming the precipitate.

During subsequent interactions, the dislocation experiences resistance from the inclusion, the Orowan loop's local field of stresses, and vacancies that form in the system. This results in an increase in stress. The average level of stresses in the system in Fig. 2 grows upon moving from s-θ' to f-θ', and then to h-θ' and (h + r)-θ'.

Figures 2e–2h show the stresses for all types of precipitates, averaged over the region and depending on the temperature. A drop in stress as the temperature rises is observed for all types of the considered precipitates. The tendency for stress to grow upon changing the type of precipitate from s-θ' to f-θ', and then to h θ' and (h + r)-θ', continues on average.

Our results from MD modeling show that systems with s-θ' and f-θ' display the average level of shear stresses in the system: 320–340 MPa. This value is 400–420 MPa for the h-θ' and (h + r)-θ' hybrid precipitates. To explain this phenomenon, we estimated local shear stresses acting on inclusion atoms lying in the dislocation slip plane (Fig. 3).

A central region containing 20 atoms was chosen in the precipitate volume (Fig. 3e). Local stresses grow during the initial interactions with a dislocation for both types of inclusions. Local stresses for s-θ' reach a maximum of around 2.6 GPa during the fourth interaction (Fig. 3a). The local stress for f-θ' is 2.9 GPa during the sixth interaction (Fig. 3b). The maximum value of local shear stresses for the h-θ' and (h + r)-θ'-type structures is approximately 4.9 GPa, which is reached during the seventh interaction (Figs. 3c, 3d). The overcutting stress thus grows by around a factor of two for the h-θ' and (h + r)-θ' hybrid phases. The local stresses acting on the inclusions and the region-averaged stresses differ by an order of magnitude. This large difference in stress is due to two factors. First, the shear stiffness of an inclusion is many times greater

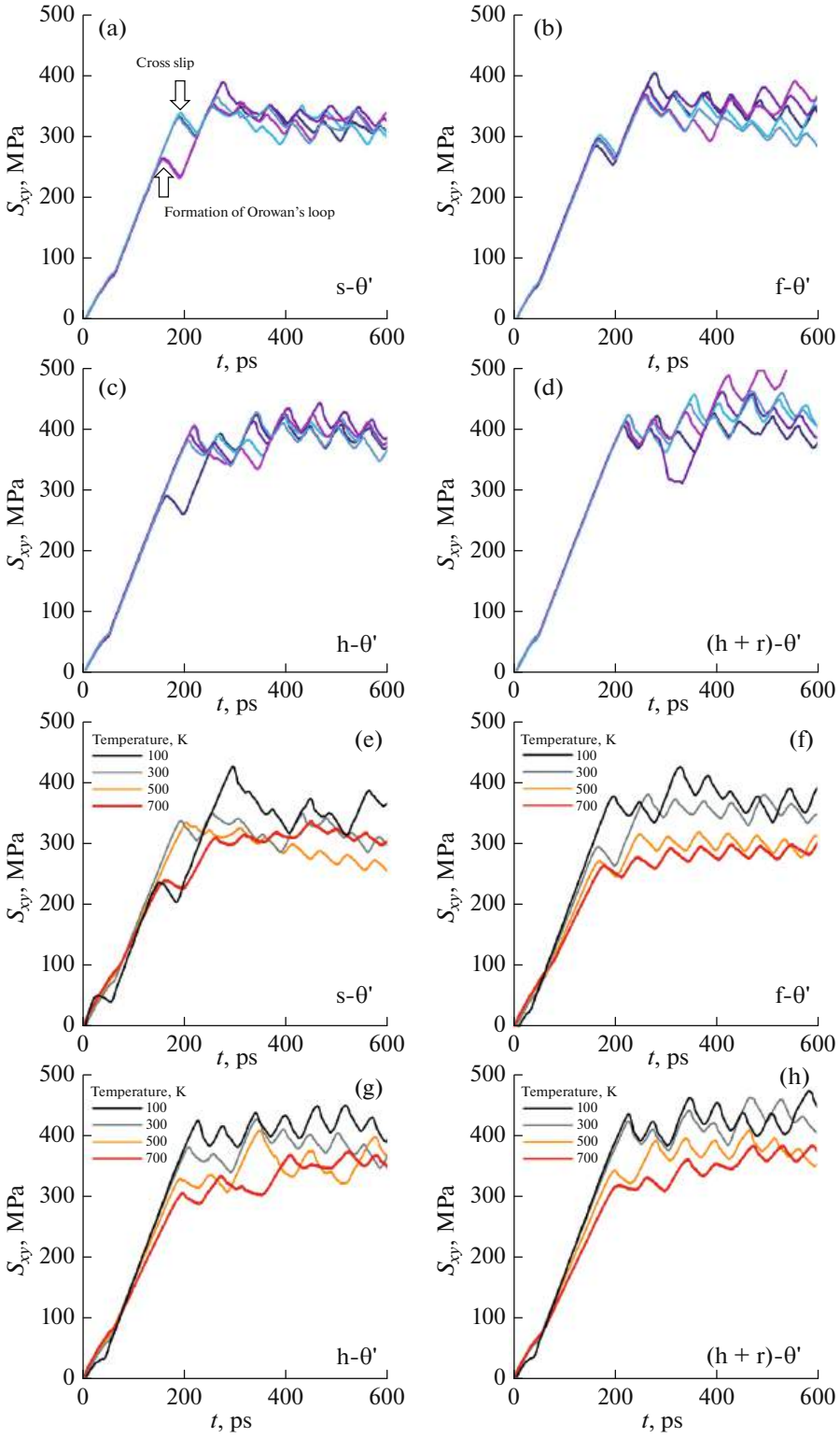

Fig. 2. System-averaged shear stresses: (a–d) statistical spread and (e–h) temperature dependence.

than that of an aluminum matrix, which allows high local stresses to accumulate during successive interactions with dislocations. Second, high local stresses have little effect on the system-averaged stresses, due to the small volume fraction of the precipitate. Local shear stresses accumulate with successive interactions between a dislocation and an inclusion, leading to its overcutting. The h-θ' and (h + r)-θ' structures are dis-

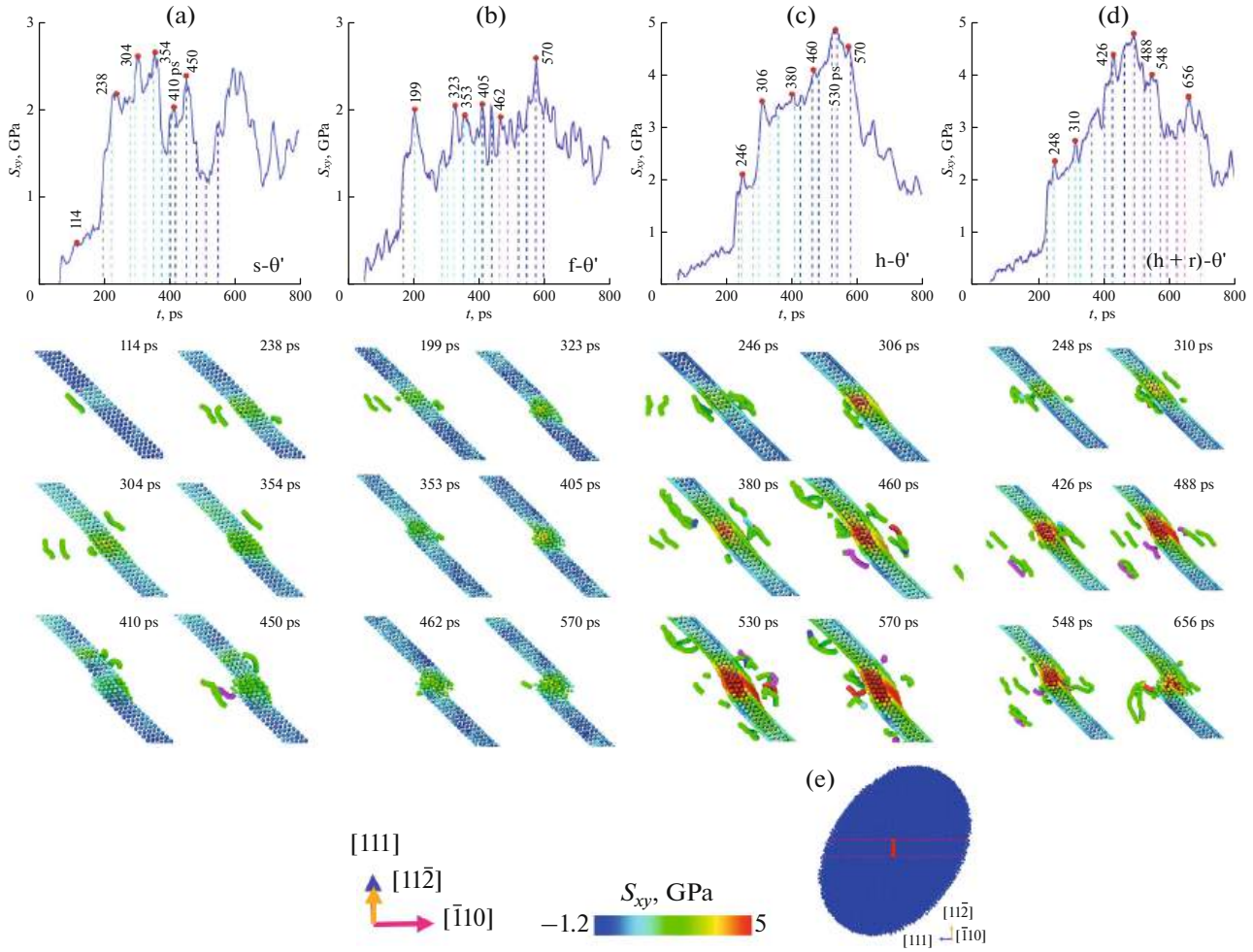

Fig. 3. Local shear stresses.

torted after several passages of dislocation but retain an ordered structure much longer, testifying to the higher shear resistance relative to the s-θ' and f-θ' structures. The critical local shear stress for s-θ' 2.2 nm thick was calculated in [26]: 2.8 GPa. In this work, the maximum local shear stress for s-θ' at an inclusion thickness of 1.4 nm was 2.6 GPa. The dependence of the cutting stress for s-θ' on its thickness was found with a proportionality factor of 0.25 GPa/nm.

We used our MD results to calibrate the continuum model of interaction between dislocations and hardening phases, based on the formation of an Orowan loop around an inclusion. The MD modeling data show that the mechanism of Orowan interaction is observed for all types of precipitates. A model for the formation of an Orowan loop based on MD calculations was proposed in [26] and refined in [15]. The difference between the types of precipitates is directly related to the change in the energy of dislocation segments adjacent to the inclusion. This energy depends on the details of the dislocation-precipitate interaction, which are determined at the atomic level by the structure of the latter. We therefore use this energy as a constant parameter for each type of precipitate, fitting it to the MD data according to the dependences of the time-averaged stress. A detailed description of the model used in this work can be found in [15]. The stress vs. time dependences obtained in accordance with the above approach are shown in Fig. 4. MD data for 300 K were used for purposes of comparison. The modeling results are in good agreement with the behavior of the mean stress in the MD system. At room temperature, the dislocation segment energies are 0.8 and 0.96 eV/b for s-θ' and f-θ'; 1.1 and 1.23 eV/b for h-θ' and (h + r)-θ', respectively, where b is the absolute value of the Burgers vector of an ideal dislocation in aluminum matrix. Other parameters of the model are given in [15, 16]. The energy of dislocation segments adjacent to hardening phases was found to be approximately 40% higher in hybrid h-θ' and (h + r)-θ' phases, due to their higher shear resistance.

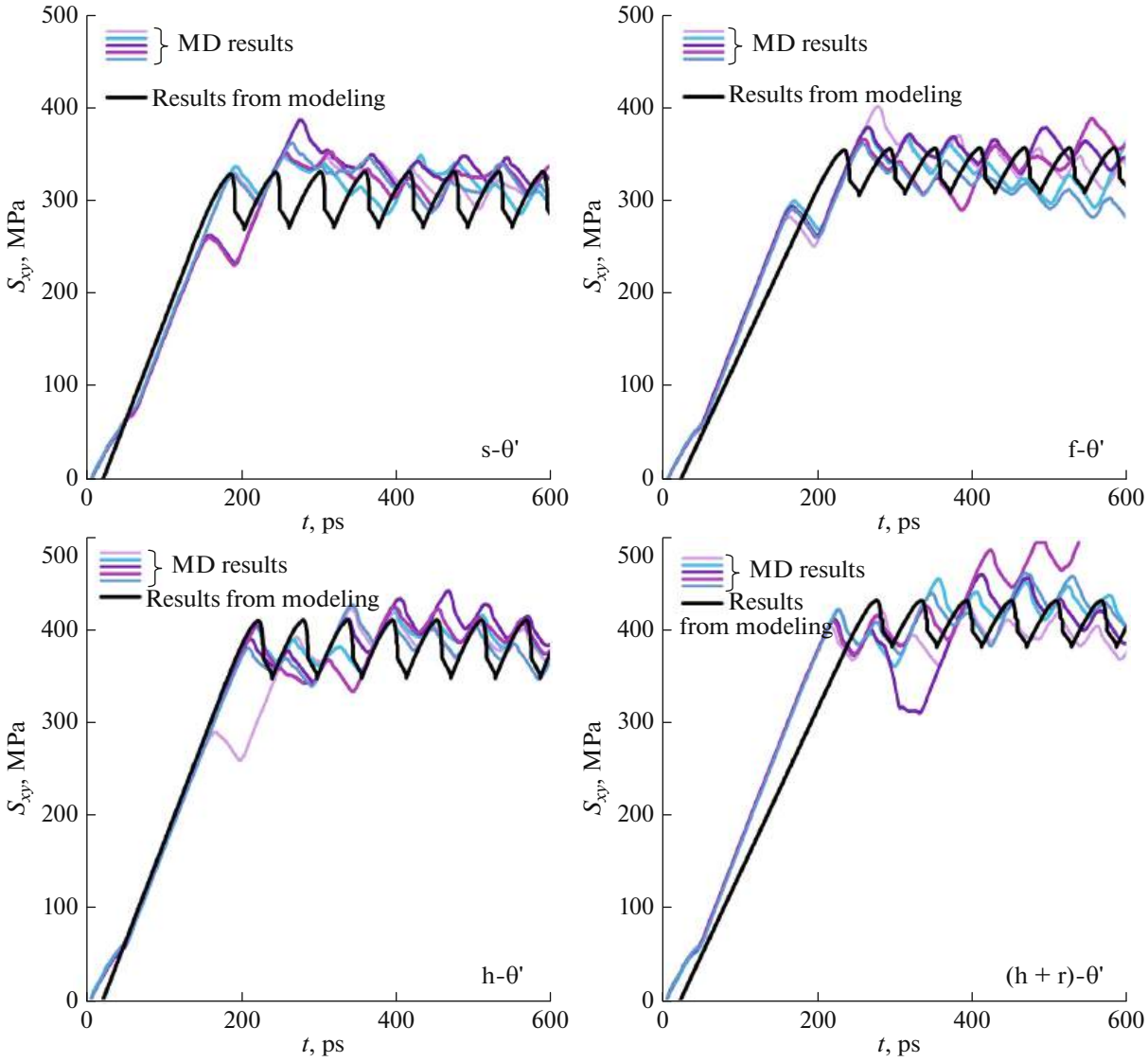

Fig. 4. Average stress in the systems. Comparison of model and MD results.

CONCLUSIONS

Molecular dynamics was used to study the shear strength of aluminum systems with four types of hardening precipitates observed in real alloys. The hybrid precipitates were found to be characterized by higher resistance to shear deformation, relative to the considered single-phase precipitates. In the continuum model proposed earlier, we determined the energy parameters for all types of structures in a wide range of temperatures. Results from MD calculations were in qualitative agreement with our data from continuum modeling.

FUNDING

This work was supported by the Russian Science Foundation, project no. 18-71-10038.

CONFLICT OF INTEREST

The authors declare that they have no conflicts of interest.

REFERENCES

1. Polmear, I.J., *Light Metals: From Traditional Alloys to Nanocrystals*, Oxford: Butterworth-Heinemann, 2006, 4th ed.
2. McDowell, D.L., *Int. J. Plast.*, 2010, vol. 26, p. 1280.
3. Kovalevskaya, T.A. and Daneyko, O.I., *Bull. Russ. Acad. Sci.: Phys.*, 2021, vol. 85, no. 7, p. 776.
4. Varyukhin, V.N. and Malashenko, V.V., *Bull. Russ. Acad. Sci.: Phys.*, 2018, vol. 82, no. 9, p. 1101.
5. Porter, D.A., Easterling, K.E., and Sherif, M.Y., *Phase Transformations in Metals and Alloys*, New York: CRC, 2014.

6. Konno, T.J., Hiraga, K., and Kawasaki, M., *Scr. Mater.*, 2001, vol. 44, nos. 8–9, p. 2302.
7. Gao, L., Li, K., Ni, S., et al., *J. Mater. Sci. Technol.*, 2021, vol. 61, p. 25.
8. Costa, TeixeiraJ., Cram, D.G., Bourgeois, L., et al., *Acta Mater.*, 2008, vol. 56, no. 20, p. 6109.
9. Chen, Y., Zhang, Z., Chen, Z., et al., *Acta Mater.*, 2017, vol. 125, p. 340.
10. Ma, Z., Zhan, L., Liu, C., et al., *Int. J. Plast.*, 2018, vol. 110, p. 183.
11. Liu, H., Papadimitriou, I., Lin, F.X., LLorca, J., et al., *Acta Mater.*, 2019, vol. 167, p. 121.
12. Zhou, L., Wu, C.L., Xie, P., et al., *J. Mater. Sci. Technol.*, 2021, vol. 75, p. 126.
13. Bourgeois, L., Medhekar, N.V., Smith, A.E., et al., *Phys. Rev. Lett.*, 2013, vol. 111, p. 069901.
14. Liu, C., Ma, Z., Ma, P., et al., *Mater. Sci. Eng., A*, 2018, vol. 733, p. 28.
15. Krasnikov, V.S., Mayer, A.E., Pogorelko, V.V., et al., *Int. J. Plast.*, 2020, vol. 125, p. 169.
16. Krasnikov, V.S., Mayer, A.E., and Pogorelko, V.V., *Int. J. Plast.*, 2020, vol. 128, p. 102672.
17. Fomin, E.V., Mayer, A.E., and Krasnikov, V.S., *Int. J. Plast.*, 2021, vol. 146, p. 103095.
18. Mahata, A. and Zaeem, M.A., *J. Cryst. Growth*, 2019, vol. 527, p. 125255.
19. Haapalehto, M., Pinomaa, T., Wang, L., and Laukkanen, A., *Comput. Mater. Sci.*, 2022, vol. 209, p. 111356.
20. Hirel, P., *Comput. Phys. Commun.*, 2015, vol. 197, p. 212.
21. Daw, M.S., Foiles, S.M., and Baskes, M.I., *Mater. Sci. Rep.*, 1993, vol. 9, p. 251.
22. Berendsen, H.J.C., Postma, J.P.M., and van Gunsteren, W.F., *J. Chem. Phys.*, 1984, vol. 81, p. 8.
23. Plimpton, S., *J. Comput. Phys.*, 1995, vol. 117, p. 1.
24. Apostol, F. and Mishin, Y., *Phys. Rev. B*, 2011, vol. 83, p. 054116.
25. Stukowski, A., *Modell. Simul. Mater. Sci. Eng.,* 2010, vol. 18, p. 015012.
26. Krasnikov, V.S. and Mayer, A.E., *Int. J. Plast.*, 2019, vol. 119, p. 21.

Translated by G. Dedkov